doi:10.1006/geno.2002.7009 **Article**

Genetic and Comparative Mapping of Genes Dysregulated in Mouse Hearts Lacking the *Hand2* Transcription Factor Gene

Melissa P. Villanueva,[1,*] Aparna R. Aiyer,[2] Shaine Muller,[2] Mathew T. Pletcher,[1] Xiao Liu,[1] Beverly Emanuel,[3] Deepak Srivastava,[2] and Roger H. Reeves[1,†]

[1]*Department of Physiology, Johns Hopkins University School of Medicine, Baltimore, Maryland 21205*
[2]*University of Texas Southwestern Medical Center, Dallas, Texas 75235-9148*
[3]*Children's Hospital of Philadelphia, Philadelphia, Pennsylvania*

**Current address: Department of Developmental Genetics, NYU Medical Center, Skirball Institute, 4th Floor, Room 2, 540 First Avenue, New York, NY 10016.*

[†]*To whom correspondence and reprint requests should be addressed at The Johns Hopkins University, School of Medicine, 725 North Wolfe Street, Baltimore, MD 21205-2105. Fax: (410) 614-8731. E-mail: rreeves@jhmi.edu.*

The helix-loop-helix transcription factor HAND2 plays a vital role in the development of the heart, limb, facies, and other neural crest-derived structures. We used differential display analysis to identify 33 putative HAND2-regulated ESTs that are differentially expressed in *Hand2*$^{-/-}$ vs wild-type mice. We determined the positions on mouse and human genetic maps of 29 of these by using the T31 mouse Radiation Hybrid panel, comparison to human genomic sequence, and comparative mapping. We examined the conserved chromosomal locations for phenotypes that involve development of heart, face, and limb structures that are affected by HAND2. One EST mapped to a region of conserved synteny between mouse chromosome 2 and human chromosome 10p. RACE analysis extended the sequence and identified this cDNA as the mouse ortholog of human nebulette, an actin-binding protein expressed in fetal heart. Nebulette was shown to be deleted in DiGeorge Syndrome 2 patients with the proximal deletion of human 10p13–p14 that is associated with cardiac and craniofacial abnormalities.

INTRODUCTION

Hand2, the gene encoding the basic helix-loop-helix transcription factor, HAND2, is expressed throughout prenatal development in the deciduum, heart, autonomic nervous system, and other neural crest-derived structures [1]. HAND2 is one of the earliest cardiac chamber-specific transcription factors identified to date [2]. By 9.5 days postcoitum (dpc) in the mouse embryo, HAND2 is expressed in the ventricular region, with abundant transcripts also in the outflow tract (conotruncus) and the first and second aortic arch arteries [1]. At 10.5 dpc, HAND2 is highly expressed in the first branchial arch (which gives rise to the craniofacial mesenchyme), the aortic sac, the third and fourth aortic arch arteries, and the truncus arteriosus [1]. HAND2 is also expressed in the limb bud where it plays a role in anterior–posterior polarization [3]. The same studies showed that ectopic expression of HAND2 results in the shortening and broadening of the long bones of the forearms and digits and preaxial polydactyly.

Mice homozygous for a null allele of *Hand2* die from heart failure by 11 dpc [2]. Heart defects in the null embryos include lack of aortic arch arteries, a dilated aortic sac, and an abrupt connection between the outflow tract and the left ventricle, due to the absence of the right ventricle [2]. In these embryos, the first and second branchial arches become hypoplastic, most likely the result of extensive apoptosis, and the third and fourth branchial arches fail to form [4]. The lack of a critical amount of neural crest cells in the third and fourth branchial arches is thought to result in persistent truncus arteriosus (failure of septation of ascending aorta and pulmonary trunk) and interruption of the aorta, which are characteristic of DiGeorge syndrome (DGS)/velocardiofacial syndrome, also known as the 22q11 deletion syndrome [5]. In addition, *Hand2*$^{-/-}$ mice demonstrated abnormal vascular development in the embryo and the yolk sac [6].

Recent investigations of the molecular basis for DGS have shown that deletions of both copies of the *Tbx1* or the *Crkol* gene in mouse disrupts development of the heart, thyroid, parathyroids, and craniofacial structure in patterns reminiscent of DGS [7–10]. Segmental monosomy for a 1.5-Mb re-

0888-7543/02 $35.00

doi:10.1006/geno.2002.7009

gion of mouse Chr 16 corresponding to most of the DGS region of Chr 22 produces these effects in a genetic model of the haploinsufficiency of DGS. Cardiac anomalies are largely reversed when a second copy of *Tbx1* is added back to the segmentally monosomic mouse [9], demonstrating a key role for this gene in this component of the DGS phenotype. However, the full complement of genetic interactions that are perturbed to produce the multiple phenotypes that characterize DGS remains to be elucidated.

In a previous study, characterization of ESTs differentially expressed in mice with or without a functional *Hand2* gene demonstrated alteration of the expression of *Ufd1l* [11]. The *Saccharomyces cerevisiae* homolog, *ufd1,* is involved in degradation of ubiquitinated proteins. Ablation of yeast *ufd1* disrupts cell survival and this perturbation is only partially reversed when a single copy of the gene is restored [12]. Human *UFD1L* maps to a region frequently deleted in DGS and thus was considered a candidate for associated anomalies based on dosage sensitivity, regulation by HAND2, pattern and timing of expression, and chromosomal position [11]. In this study, we determined the map positions in mouse and human of 29 additional genes whose expression may be altered in hearts of *Hand2*$^{-/-}$ mice (A. Aiyer and D. Srivastava, in preparation) and compared these positions to mapped phenotypes including arrhythmogenic right ventricular dysplasia, dilated cardiomyopathy, cardiofaciocutaneous syndrome, and DGS. One of these is demonstrated to be the mouse ortholog of nebulette (*NEBL*), an actin-binding protein expressed primarily in the heart. *NEBL* transcripts have been isolated from human embryonic heart and early mouse fetuses. The gene localizes to the DiGeorge syndrome 2 (DGS2) region on human chromosome 10p14–p13. Here we refine that localization with respect to the portion of the DGS2 deletion region that is correlated with cardiac defects, as opposed to the region of segmental monosomy in individuals with the hypoparathyroidism, deafness, and renal dysplasia (HDR) spectrum of anomalies.

RESULTS

Mapping of ESTs

Twenty-nine ESTs isolated through differential display analysis (DDA sequences) or subtractive hybridization (RDA sequences) were unique. We developed primers from these, and 22 of them were mapped with high confidence (lod scores ranging from 6.1 to 25.6) on the T31 mouse Radiation Hybrid (RH) panel (Table 1 and http://www.jax.org/resources/documents/cmdata/rhmap/RHIntro.html). One transcript, DDA34, represents the mouse gene, *Enolase2* (*Eno2*), which was mapped previously to chromosome 6, map position 60.21, by backcross and physical mapping. We mapped *Eno2* on the RH panel to mouse chromosome 6 between 57 and 60 map units to validate the RH mapping procedures. DDA38, which represents mouse *Kcnq1,* was mapped previously to chromosome 7, map position 69.3, by backcross and physical mapping. The human ortholog, *KCNQ1,* has been located on human chromosome 11p15.5. We mapped *Kcnq1* to distal mouse chromosome 7, between 71 and 72 map units. Nine additional ESTs corresponded to genes mapped previously in mouse or human (Table 2). Twenty-one of the 22 mapped ESTs were localized to mouse chromosomal regions with an interval size <4 map units (Table 1).

We initially used comparison of mouse and human genetic maps to predict the most likely locations in both mouse and human genomes of orthologous genes (Table 1) (see Materials and Methods). Of the 22 ESTs mapped by the RH panel, 18 had an unambiguous predicted human location and 4 mouse positions did not discriminate between two possible locations in the human genome (Table 1). To resolve some of these ambiguities, we compared the DDA sequences by BLAST to human and mouse genomic sequence. No matches were found to publicly available mouse genomic sequence. However, 15 of them detected one or more significant human matches, and 14 of these matched the predicted chromosomal location with the highest homology score, refining and confirming predictions from comparative mapping. The 7 sequences that could not be mapped on the RH panel had strong hits in human sequence, such that comparative mapping predicted the mouse genomic location. One sequence, RDA30, mapped to a position on mouse Chr 4 that predicted a human ortholog on human chromosome 9p21–p22, but this sequence detected human genomic sequence matches on chromosomes 6 and 11 (Table 1). Mouse Chr 4 contains a small segment of chromosome 6 homology located between conserved syntenies with human chromosomes 8 and 9. RDA30 may represent a gene from a segment that is separated from the few other human chromosome 6 genes on this mouse chromosome, or the gene order may be incorrect on the composite mouse map. Mouse genome sequencing will resolve this issue.

DDA Sequence Expression and Mapped Phenotypes

Twenty-two unique sequences from the differential display analysis could be shown independently to be transcribed sequences based on expression studies or EST matches (Table 2). Twelve of these matched known mouse genes and/or their human orthologs. We identified and mapped a number of these for the first time in mouse or human. Nine DDA sequences matched sequences in "full-length-enriched" Riken cDNA libraries [13]. Six were confirmed to occur in heart and/or early embryo.

We identified phenotypes in humans and mice that map near to each EST position in OMIM and MGD (Table 1). Anomalies that involve the heart, vascular system, limb, facies, and neural crest-derived structures might be consistent with the known effects of HAND2. In addition, effects on melanocytes, calcitonin-secreting cells, and the adrenal gland could arise as a result of the loss of HAND2 expression affecting neural crest development and migration [11]. Several DDA sequences mapped to the same chromosomal

TABLE 1: EST RH Mapping Results, Mouse/Human Map Positions, and Phenotypes Associated with Map Positions

Name of EST	Best fit on RH panel (proximal marker-distal marker)	Mouse chromosome (map position)	Predicted human map position	Human genomic sequence matches	Phenotypic associations in mouse and human (M, mouse, and H, human)
DDA5	—	18 (1)	10p11, 8q	10p11.23	
DDA7	—	4 (57.4)	1p35–p34	1p34.2	M: snubnose (98332) H: Schwartz–Jampel syndrome (255800)
DDA8	—	9 (15–30)[a]	11q23.3	11q23.3	M: variable spotting (98939), luxoid (96851) H: Jacobsen syndrome (147791), hydrolethalus syndrome (236680)
DDA9	—	10 (7–29)[a]	6q23	6q23.3 and 5q22.1	M: gray-lethal (95725) H: cardiomyopathy (602067)
DDA14	*D1Mit415–D1Mit49*	1 (52–55)	2q37	—	H: brachydactyly–mental retardation (600430), brachydactyly (113300)
DDA16	*D16Mit157–D16Mit169*	16 (34–37)	3q28–q29 or 3p11	—	
DDA17	*D19Mit57–D19Mit39*	19 (24)	10q23–q24 or 9p24	—	H: split hand/foot malformation (600095)
DDA21	—	8 or 14[a]	8p23.1	8p23.1[b]	
DDA22	*D4Mit91–D4Mit214*	4 (15–18)	9p21–p13	—	M: crinkly tail (88573) H: arthrogryposis multiplex congenita (108120), cartilage-hair hypoplasia (250250), acromesomelic dysplasia (602875)
DDA23	*D2Mit267–D2Mit464*	2 (8–9)	10p11–13	—	M: Danforth's short tail (98265) H: DiGeorge/velocardiofacial syndrome (601362), arrhythmogenic right ventricular dysplasia (604401)
DDA24	*D4Mit31–D4Mit146*	4 (51–54)	1p33–p32.1	1p32.1–p33	
DDA25	*D18Mit183–D18Mit107*	18 (37)	18p11.2	18p11.21	
DDA26	—	12 or 14[a]	14q11.2–q12	14q12[b]	H: Arrhythmogenic right ventricular dysplasia (602086)
DDA27	*D3Mit355–D3Mit154*	3 (33)	3q25–q26 or 4q32–q33	3q25.33	H: Cornelia De Lange syndrome (122470)
DDA28	*D5Mit336–D5Mit356*	5 (41)	4p14–p12	4p11	M: recessive spotting (98188), rump white (98213), patch (97571) H: total anomalous pulmonary venous return (106700)
DDA29	—	5 (B and F)	12q23–q24.1	12q24.11[b]	H: Darier disease (124200)[g], brachydactyly (113100), cardiofaciocutaneous syndrome (115150)
DDA30	*D9Mit51–D9Mit310*	9 (61)	3p24–p21	—	H: cardiomyopathy (601154), arrhythmogenic right ventricular dysplasia (604400)
DDA31	*D10Mit60–D10Mit258*	10 (30–31)	10q22	—	M: gray-lethal (95725)
DDA33	*D19Mit5–D19Mit12*	19 (26–34)	10q23–q24	—	M: hemoglobin deficient (96028) H: split hand/foot malformation (600095)
DDA34	*D6Mit134–D6Mit255*	6 (57–60)	12p13	12p13.31[b]	H: acrocallosal syndrome (200990)
DDA35	*D14Mit134–D14Mit132*	14 (1–3)	3p14 or 10q21–q24	—	M: talipes (98479) H: cardiomyopathy (601493), Moebius syndrome (604185), split hand/foot malformation (600095)

doi:10.1006/geno.2002.7009

TABLE 1: Continued

Name of EST	Best fit on RH panel (proximal marker-distal marker)	Mouse chromosome (map position)	Predicted human map position	Human genomic sequence matches	Phenotypic associations in mouse and human (M, mouse, and H, human)
DDA38	*D7Mit177–D7Mit15*	7 (71–72)	11p15.5	—	M: earlier X zone degeneration (95463) H: Jervell and Lange–Nielsen syndrome (220400), QT syndrome (192500)
DDA45	*D16Mit4–D16Mit59*	16 (27–28)	3q13–q21	—	H: Moebius syndrome (601471), Charcot–Marie–Tooth neuropathy (600882)
DDA46	*D10Mit99–D10Mit71*	10 (60–61)	12q21	—	
DDA47	*D2Mit245–D2Mit219*	2 (43–44)	2q31–q32	2q31.2 and 10q11.21[b]	H: cardiomyopathy (604145), arrhythmogenic right ventricular dysplasia (602087)
DDA49	*DXMit81–DXMit49*	X (9–13)	Xq22–q24	—	M: wide-faced (1310006) H: Miles–Carpenter syndrome (309605), Alport syndrome (300195)
DDA50	*D3Mit62–D3Mit28*	3 (4–6)	8q13–q22	—	
RDA30	*D4Mit327–D4Mit245*	4 (42)	9p22–p21	6p24.1 and 11q13.4	M: pintail (97790) H: arthrogryposis multiplex congenita (108120), orofacial cleft 1 (119530)
RDA32	*D7Mit220–D7Mit328*	7 (52–54)	11p15	11p15.3	H: arthrogryposis multiplex congenita (601680)

The best fit for each EST mapped on the RH panel was between two MIT markers. ESTs not mapped by the RH panel are indicated by a dash (—) in the second column. Mouse and/or human map positions for these ESTs are based on known map positions or comparative mapping. Map positions in mouse are specified by distance from the mouse centromere in map units on the MGI consensus linkage map. Phenotypic associations in mouse and human are indicated by Mouse Genome Database (MGD) identification numbers and Online Mendelian Inheritance in Man (OMIM) identification numbers, respectively.

[a] Position in mouse predicted based on the chromosomal location of the best human match.

[b] Sequence showed homology to other chromosomal segments with lower but still significant scores.

regions as phenotypes affecting the heart, such as arrhythmogenic right ventricular dysplasia (DDA23, 26, 30, 47), other cardiomyopathies (DDA9, 35, 47), and QT syndrome (DDA38). Two ESTs mapped in human chromosomal regions associated with syndromes that involve both congenital heart defects and craniofacial defects. The human ortholog of DDA29 mapped to HSA 12q24.11, the same region as cardiofaciocutaneous syndrome, while DDA23 mapped to the region responsible for DGS2 on HSA10. We characterized DDA23 further.

DDA23 Is the Mouse Ortholog of Nebulette (*NEBL*)

Comparative mapping predicted that the human ortholog of DDA23 would be located on 10p14–p13. Haploinsufficiency for this region of HSA 10 results in a clinical presentation of DiGeorge syndrome [14,15]. The short DDA23 sequence (448 bp) did not match known genes or ESTs. However, extension of the sequence using 5′ and 3′ rapid amplification of cDNA ends (RACE) identified significant homology to human *NEBL* (Table 2). The open reading frame of human fetal *nebulette* encodes a 115-kDa cardiac actin-binding protein that shares homology with human skeletal muscle nebulin [16,17].

The current study identifies *nebulette* (as DDA23) from E9.5 mouse heart. *nebulette* has been identified previously in cDNA libraries of human fetal heart (HSY17673) and embryonic day 13 mouse heart (BB658903). To confirm expression in fetal heart, we performed RT-PCR on mRNA from E9.5 mouse hearts. A *nebulette* product was obtained from both wild-type and *Hand2*$^{-/-}$ hearts. Amplification using equal starting amounts of RNA showed a consistent reduction of about fourfold in *nebulette* product from *Hand2*$^{-/-}$ hearts after 18, 20, 22, or 24 cycles of PCR.

Mapping of Human *nebulette* Using Fluorescence *in Situ* Hybridization (FISH)

Previous gene mapping studies indicated that human *nebulette* is mapped to chromosome 10p12 [18]. To identify more precisely the location of *NEBL* in relation to the DGS2 region, we examined cell lines with 10p deletions by FISH using overlapping BACs that contain the gene (Fig. 1). The BACs were absent from two of the deleted cell lines, CH95-199 and GM03470. CH95-199 was derived from a female with a cardiac defect, immune deficiency, cleft palate, facial dysmorphia, and developmental delay [19]. GM03470 was derived from a female with microcephaly, microphthalmia, and hypotelorism. The BACs were not deleted from the GM06936 or CH92-092 cell lines, which were derived from patients who had hypocalcemia, immune defect, developmental delay, and renal or genitourinary anomalies (hypoplasia and ureteral reflux, respectively). Neither of these individuals had a cardiac defect. Thus, their features were consistent with the HDR spectrum of DGS2 anomalies. The

TABLE 2: Transcript Alignments of DDA and RDA Sequences

Mouse EST	Transcript alignments [accession number]	Expect value	Expressed in heart	Expressed in embryo
DDA5	Kinesin family member 5B (*Kif5b*) [NM_008448]	e-147	X	X
DDA7	Microtubule-actin crosslinking factor (*Aclp7*) [AF150755]	e-167	X	
DDA8	Ubiquitin-specific protease (*Usp2*) [AF079565]	2e-65		
DDA9	*Homo sapiens* Bcl-2-associated transcription factor [AF249273]	e-135	X	
DDA14	RIKEN full-length clone 5730526A02 (from 8-day embryo) [AV305124]	e-100		X
DDA17	RIKEN full-length clone A530087E01 (from adult male aorta) [BB224579]	e-131	X	
DDA21	RNA pol II transcriptional coactivator (*Rpo2tcI*) [NM_011294]	0		
DDA23	*Homo sapiens* Nebulette (*NEBL*) [AF047368]	None[a]	X	X
DDA24	Tetratricopeptide repeat domain 4 (*Ttc4*) [AF177029]	0		
DDA25	Mouse 8.5-dpc whole embryo cDNA [BM249163]	0		X
DDA26	*BCL2*/adenovirus E1B 19-kDa-interacting protein 3 (*Bnip3*) [NM_009760]	0	X	
DDA27	RIKEN full-length clone 1110032F04 (from 18-day embryo) [AK004029]	e-123		X
DDA28	RIKEN full-length clone 6030432N09 [NM_023429]	e-165		
DDA29	Sarco/endoplasmic reticulum Ca^{2+} ATPase (*SERCA2*) [AJ131870]	e-157	X	
DDA30	RIKEN full-length clone, 9.5-day embryo parthenogenote [BB294262]	0		X
DDA34	γ-neuronal enolase (*Eno2*) [NM_013509]	e-143		
DDA38	Partial *Kcnq1* gene for potassium channel protein [AJ271885]	e-113	X	X
DDA45	Mouse EST from 13-day embryo [AV165138]	0		X
DDA46	RIKEN full-length clone A630014C11 [BB228450]	e-106		
DDA47	RIKEN full-length clone 2610209F03; myotubularin related	e-123	X	
DDA49	Multiple mouse ESTs and RIKEN clones [AA408993, BB552273, AV255749]	0		X
DDA50	RIKEN full-length clone 4930431H11 [AK015268]	2e-89		
RDA32	RIKEN full-length clone C630020M02 [BB653272]	0		
RDA30	RIKEN full-length clone 1810030E20 [AK007653]	0		X

DDA23 did not share any significant homology with human *NEBL*, and there is no mouse nebulette cDNA sequence in the GenBank database. The extended RACE product of DDA23 shared significant homology with human *NEBL*.

BAC was present on the der(10) in GM10207, which narrows the gene location to the interval shown in Fig. 1.

DISCUSSION

HAND2 plays an important role during development, and genes expressed downstream of it may be candidates for anomalies of the heart, vascular system, facies, limb, and various neural crest-derived structures. In this study, genes whose expression was affected in hearts of *Hand2*$^{-/-}$ mice, as determined by differential display, were mapped to several chromosomal regions linked to phenotypes judged to be consistent with the known effects of HAND2. One gene in particular, human *nebulette*, is expressed in early heart development and maps to the candidate region for heart defects in DiGeorge Syndrome 2 on HSA 10p.

Several of the putative HAND2-dependent genes identified here have vital functions in development. The targeted disruption of *Kif5b* (DDA5) results in embryonic lethality in the mouse, with severe growth retardation at 9.5–11.5 dpc [20]. *Kif5b* is essential for mitochondrial and lysosomal dispersion [20]. *Usp2* (DDA8) is a ubiquitin-specific protease, inhibition of which may result in apoptosis in cells of the developing heart [11].

Several genes that show significant sequence similarity to the ESTs obtained by differential display have abundant transcripts in the heart. *Kcnq1*, represented by DDA38, is expressed during mouse development, beginning at embryonic day 9.5, within the atrial and ventricular myocardium [21]. *Aclp7*, which shares significant sequence similarity with DDA7, is an actin-binding protein that is expressed mainly in the lung, brain, spinal cord, and skeletal and cardiac

doi:10.1006/geno.2002.7009

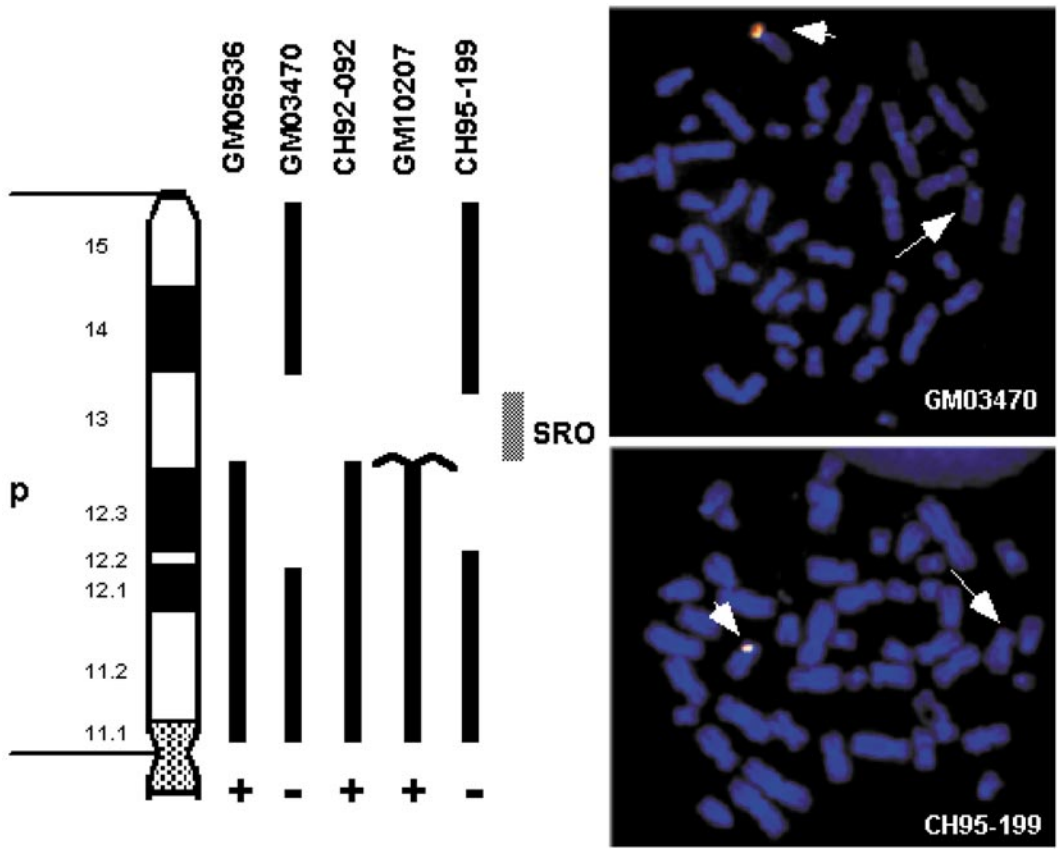

FIG. 1. Mapping the *NEBL* gene by FISH. (Left) Chromosomal idiogram with black rectangles alongside indicating the portion of 10p present in the cell lines. In the case of GM10207, only the der(10) is indicated. The presence of a plus sign below the idiogram indicates whether the BACs gave a positive signal on the deleted or der(10) by FISH analysis. A minus sign indicates the BACs were deleted. The SRO in gray indicates the smallest region of deletion overlap for the location of the *NEBL* gene. (Right) Representative FISH images. The shorter arrow indicates the normal chromosome with overlapping signals from the FITC-(BAC 56H7) and rhodamine- (BAC45L12) labeled *nebulette*-containing BACs. The longer arrow indicates the deleted chromosome 10. Chromosome identification was accomplished by converting the DAPI-counterstained image to gray scale.

muscle [22]. This gene mapped to the same human chromosomal region as Schwartz–Jampel syndrome (Table 1), which includes facial abnormalities consistent with the *Hand2*$^{-/-}$ expression pattern. Many phenotypes mapped to the same regions, as HAND2-dependent ESTs were characterized by anomalies in structures other than heart that have been shown to express HAND2 during development, e.g., the limb and facies (Table 1). Finally, HAND2 may play a role in neural crest differentiation and migration. The mouse mutant phenotypes *recessive spotting, rump white,* and *patch deletion region,* which involve neural crest-derived melanocytes, map on MMU5 near DDA28.

Four ESTs mapped near regions linked to dilated cardiomyopathy (Table 1). Two of these loci (represented by DDA30 and 47) are also linked to arrythmogenic right ventricular dysplasia (ARVD). DDA47 matches a RIKEN full-length clone (Table 2) that is closely related to myotubularin (*Mtm1*) and myotubularin-related (*Mtmr1*) genes (GenBank Accession No. AF125314, e-103). Mutations in myotubularin have been linked to dilated cardiomyopathy [23–25]. *KCNQ1*, the human ortholog of DDA38, mapped to a chromosomal region linked to syndromes characterized by cardiac arrhythmias, Long QT syndrome (LQTS) and Jervell and Lange–Nielsen syndrome (JLNS). It has been proposed that mutations in *KCNQ1* provide a molecular basis for the cardiac arrhythmias seen in LQTS and JLNS [26–28].

Two ESTs mapped to loci responsible for congenital diseases that demonstrate anomalies of the heart and craniofacial structures. The human ortholog of DDA29, *ATP2A2,* localizes to a chromosomal region characterized by cardiofaciocutaneous syndrome. Patients with this syndrome commonly exhibit pulmonic stenosis, atrial septal defect, and characteristic facial appearance (http://www.ncbi.nlm.nih.gov/entrez/query.fcgi?db = OMIM). The *ATP2A2* gene encodes the sarco(endo)plasmic reticulum Ca^{2+}-ATPase2 (SERCA2) isoforms [29]. The ATP2A2a isoform (SERCA2a) is expressed mainly in the cardiac and skeletal muscle, and its expression and sarcoplasmic Ca^{2+} handling are decreased

in cardiac hypertrophy and in human heart failure [30]. Dysregulation of this gene in *Hand2*$^{-/-}$ mice could occur secondarily to heart failure.

Human *nebulette* maps to HSA 10p14–p13. This chromosomal region is involved in ARVD and is deleted in patients presenting cardiac defects in DGS2. Cardiac defects in DiGeorge patients result primarily from abnormal development of the branchial and aortic arch arteries, a defect that is also observed in *Hand2*$^{-/-}$ embryos. Anomalies of embryonic heart development, such as persistent truncus arteriosus and interruption of the aorta, have been detected in DiGeorge patients and are thought to be the result of abnormal development of the third and fourth neural crest-derived branchial arches and their corresponding aortic arch arteries, which are hypoplastic and lack critical growth in *Hand2*$^{-/-}$ embryos.

Different features of DiGeorge syndrome map to two regions on HSA 10p [31]. Haploinsufficiency of the more distal region can cause HDR. Deletions that involve only the more proximal region are associated with cardiac defects, cleft palate, and T cell deficiencies [31]. We demonstrated that *nebulette* was deleted in two DGS2 patients with the more proximal deletion who showed cardiac defects, but not in two patients with the more distal deletion, which is associated with HDR.

The genes mapped in this study are linked functionally to HAND2 as molecules whose expression is altered in a differential display assay of embryonic hearts with or without this transcription factor. Some may be downstream effectors of HAND2 action in heart development. Using RH mapping, comparative sequence analysis, and BLAST searches against genomic databases, we localized 29 of these products and compared their genomic locations to those of mapped phenotypes related to their expression patterns. Several of these sequences are reasonable candidates for the molecular and genetic basis of diseases that affect heart and the derivatives of neural crest, tissues that ultimately lie downstream of HAND2.

Materials and Methods

RH mapping. PCR primers were designed using Primer 3 (http://www.genome.wi.mit.edu/cgi-bin/primer/primer3.cgi) for the 22 differential display products (ESTs) whose expression was affected in E10.5 *Hand2*$^{-/-}$ embryos and that did not match previously mapped genes. Primers were purchased from Life Technologies (Gaithersburg, MD). Optimal PCR conditions for each EST were established by the successful amplification of the expected product from embryonic stem cell DNA and a different size or no product from A3 hamster DNA. The majority of mouse primers amplified one or more hamster DNA fragments. Primers and optimal PCR conditions used for radiation hybrid mapping of 22 ESTs can be found at (http://inertia.bs.jhmi.edu/roger.html). Each primer set was typed at least three times on the entire T31 RH panel (Research Genetics, Huntsville, AL). RH typings were submitted to the Jackson Laboratory Mouse Radiation Hybrid Database (http://www.jax.org/resources/documents/cmdata/rhmap/RHIntro.html) for analysis and archiving of results. This service uses Map Manager QTb28 to determine the highest lod scores for each EST mapped and the "best fit" interval where each EST is most likely localized. The markers that identify the boundaries for this interval are indicated in Table 1. RH data are publicly available at the Jackson Laboratory Mouse Radiation Hybrid Database.

Comparative mapping. The best position on the MGI Consensus Linkage Map for each EST mapped on the radiation hybrid panel was determined by comparing the positions of markers common to the RH and MGI maps. Where marker orders disagreed, the most likely marker order was deduced by comparing the RH map, the MGI consensus map (http://www.informatics.jax.org/searches/linkmap_form.shtml), the MIT F2 Intercross map (http://www-genome.wi.mit.edu/cgi-bin/mouse/index#genetic), and the Jackson BSS backcross map (http://lena.jax.org/resources/documents/cmdata/bkmap/). The most likely region of conserved synteny in the human was assigned by comparing map positions of orthologous mouse:human gene pairs from the MGI map. In many cases, this could be confirmed by searching the "complete draft" human genomic sequence from the Human Genome Project and Celera Public databases. Mouse and human phenotypes were obtained from MGI and Online Mendelian Inheritance in Man (OMIM) (http://www.ncbi.nlm.nih.gov/Omim/searchmap.html).

Characterization of EST sequences. Mouse EST sequences obtained by differential display of mRNA from the hearts of wild-type and *Hand2*$^{-/-}$ 9.5-dpc embryos [32] were masked for repeat elements (http://woody.embl-heidelberg.de/repeatmask/) and aligned to GenBank's dbest and nonredundant sequence databases (http://www.ncbi.nlm.nih.gov/BLAST) and the TIGR EST database (http://www.tigr.org/tdb/tgi/mgi/). The EST and its mouse cDNA match in BLAST were considered to be equivalent to each other if they shared ≥98% identity in nucleotide sequence (Table 2). Cognate ESTs were aligned with mouse genomic sequence using the Ensembl (http://www.ensembl.org/Mus_musculus/) or Celera (http://cds.celera.com/) database.

RACE. RACE was performed to extend the cDNA sequence of the EST DDA23. Using the TRIzol reagent (Life Technologies), total RNA was collected from 10.5-dpc embryos. 5′ RACE-Ready cDNA and 3′ RACE-Ready cDNA were synthesized using the SMART RACE cDNA amplification system (Clontech, Inc.). 5′ and 3′ cDNA products were amplified using the DDA23 radiation hybrid primers with RACE kit universal primers. RACE products were examined on 1% agarose gels. Successful RACE reactions were subcloned using the TOPO TA Cloning Kit (Invitrogen). Restriction digests verified insert sizes. Appropriate clones were sequenced and analyzed as described for other ESTs.

FISH analysis. Metaphase spreads were prepared either from peripheral blood lymphocytes or from lymphoblastoid cell lines using standard methodology. Five cell lines and two control samples were used. Three cell lines were purchased from the Coriell mutant cell repository (Camden, NJ). These included GM06936 [46,XX,del(10)(qter→p13], GM03470 [46,XX,del(10)(pter→p13::p12→qter], and GM10207 [46,XY,t(10;14)(p13;q24.3)]. CH95-199 and CH92-092, two additional cell lines used in this study, have been reported previously [19]. FISH was performed as previously described [33]. Chromosomes were visualized by counterstaining with DAPI. Probes used for FISH were labeled by nick translation with either biotin-16–dUTP or digoxigenin-11–dUTP as described [34] with minor modifications. The probes were detected by either fluorescein-conjugated avidin or rhodamine-conjugated anti-digoxigenin, respectively. The FISH probes were chromosome 10 BACs RP11-45L12 (AC012108) and 56H7 (AL157398) from the RPCI-11 human BAC library (Roswell Park Cancer Institute). These BACs contain the *nebulette* gene and were identified by searching public databases for sequenced clones using the GenBank entry for the human *nebulette* cDNA (AF047368).

Acknowledgments

This work was supported in part by awards from the March of Dimes and Smile Train (D.S.) and by PHS awards from NHLBI (D.S.), HD26979 (B.S.E.), and DC02027 (R.H.R. and B.S.E.).

References

1. Srivastava, D., Cserjesi, P., and Olson, E. N. (1995). A subclass of bHLH proteins required for cardiac morphogenesis. *Science* **270:** 1995–1999.
2. Srivastava, D., *et al.* (1997). Regulation of cardiac mesodermal and neural crest development by the bHLH transcription factor, dHAND. *Nat. Genet.* **16:** 154–160. [Published erratum appears in *Nat. Genet.*, 1997, **16:** 410]

3. Fernandez-Teran, M., *et al.* (2000). Role of dHAND in the anterior–posterior polarization of the limb bud: Implications for the Sonic hedgehog pathway. *Development* **127:** 2133–2142.
4. Thomas, T., *et al.* (1998). A signaling cascade involving endothelin-1, dHAND and msx1 regulates development of neural-crest-derived branchial arch mesenchyme. *Development* **125:** 3005–3014.
5. Kirby, M. L., and Waldo, K. L. (1990). Role of neural crest in congenital heart disease. *Circulation* **82:** 332–340.
6. Yamagishi, H., Olson, E. N., and Srivastava, D. (2000). The basic helix-loop-helix transcription factor, dHAND, is required for vascular development. *J. Clin. Invest.* **105:** 261–270.
7. Guris, D. L., Fantes, J., Tara, D., Druker, B. J., and Imamoto, A. (2001). Mice lacking the homologue of the human 22q11.2 gene CRKL phenocopy neurocristopathies of DiGeorge syndrome. *Nat. Genet.* **27:** 293–298.
8. Lindsay, E. A., *et al.* (2001). Tbx1 haploinsufficiency in the DiGeorge syndrome region causes aortic arch defects in mice. *Nature* **410:** 97–101.
9. Merscher, S., *et al.* (2001). TBX1 is responsible for cardiovascular defects in velo-cardio-facial/DiGeorge syndrome. *Cell* **104:** 619–629.
10. Jerome, L. A., and Papaioannou, V. E. (2001). DiGeorge syndrome phenotype in mice mutant for the T-box gene, Tbx1. *Nat. Genet.* **27:** 286–291.
11. Yamagishi, H., Garg, V., Matsuoka, R., Thomas, T., and Srivastava, D. (1999). A molecular pathway revealing a genetic basis for human cardiac and craniofacial defects. *Science* **283:** 1158–1161.
12. Johnson, E. S., Ma, P. C., Ota, I. M., and Varshavsky, A. (1995). A proteolytic pathway that recognizes ubiquitin as a degradation signal. *J. Biol. Chem.* **270:** 17442–17456.
13. Kawai, J., *et al.* (2001). Functional annotation of a full-length mouse cDNA collection. *Nature* **409:** 685–690.
14. Daw, S. C., *et al.* (1996). A common region of 10p deleted in DiGeorge and velocardiofacial syndromes. *Nat. Genet.* **13:** 458–460.
15. Schuffenhauer, S., *et al.* (1998). Deletion mapping on chromosome 10p and definition of a critical region for the second DiGeorge syndrome locus (DGS2). *Eur. J. Hum. Genet.* **6:** 213–225.
16. Moncman, C. L., and Wang, K. (1995). Nebulette: A 107 kD nebulin-like protein in cardiac muscle. *Cell Motil. Cytoskeleton* **32:** 205–225.
17. Moncman, C. L., and Wang, K. (1999). Functional dissection of nebulette demonstrates actin binding of nebulin-like repeats and Z-line targeting of SH3 and linker domains. *Cell Motil. Cytoskeleton* **44:** 1–22.
18. Millevoi, S., *et al.* (1998). Characterization of nebulette and nebulin and emerging concepts of their roles for vertebrate Z-discs. *J. Mol. Biol.* **282:** 111–123.
19. Gottlieb, S., *et al.* (1998). Characterization of 10p deletions suggests two nonoverlapping regions contribute to the DiGeorge syndrome phenotype. *Am. J. Hum. Genet.* **62:** 495–498.
20. Tanaka, Y., *et al.* (1998). Targeted disruption of mouse conventional kinesin heavy chain, kif5B, results in abnormal perinuclear clustering of mitochondria. *Cell* **93:** 1147–1158.
21. Franco, D., *et al.* (2001). Divergent expression of delayed rectifier K(+) channel subunits during mouse heart development. *Cardiovasc. Res.* **52:** 65–75.
22. Bernier, G., Mathieu, M., De Repentigny, Y., Vidal, S. M., and Kothary, R. (1996). Cloning and characterization of mouse ACF7, a novel member of the dystonin subfamily of actin binding proteins. *Genomics* **38:** 19–29.
23. de Gouyon, B. M., *et al.* (1997). Characterization of mutations in the myotubularin gene in twenty six patients with X-linked myotubular myopathy. *Hum. Mol. Genet.* **6:** 1499–1504.
24. Laporte, J., *et al.* (1997). Mutations in the MTM1 gene implicated in X-linked myotubular myopathy. ENMC International Consortium on Myotubular Myopathy, European Neuro-Muscular Center. *Hum. Mol. Genet.* **6:** 1505–1511.
25. Tanner, S. M., *et al.* (1999). Characterization of 34 novel and six known MTM1 gene mutations in 47 unrelated X-linked myotubular myopathy patients. *Neuromusc. Disord.* **9:** 41–49.
26. Ko, Y. L., *et al.* (2001). Linkage and mutation analysis in two Taiwanese families with long QT syndrome. *J. Formosan Med. Assoc.* **100:** 767–771.
27. Kubota, T., *et al.* (2001). Evidence for a single nucleotide polymorphism in the KCNQ1 potassium channel that underlies susceptibility to life-threatening arrhythmias. *J. Cardiovasc. Electrophysiol.* **12:** 1223–1229.
28. Schmitt, N., *et al.* (2000). A recessive C-terminal Jervell and Lange–Nielsen mutation of the KCNQ1 channel impairs subunit assembly. *EMBO J.* **19:** 332–340.
29. Ver Heyen, M., *et al.* (2000). Structure and organization of the mouse Atp2a2 gene encoding the sarco(endo)plasmic reticulum Ca^{2+}-ATPase 2 (SERCA2) isoforms. *Mamm. Genome* **11:** 159–163.
30. Arai, M., Matsui, H., and Periasamy, M. (1994). Sarcoplasmic reticulum gene expression in cardiac hypertrophy and heart failure. *Circ. Res.* **74:** 555–564.
31. Lichtner, P., *et al.* (2000). An HDR (hypoparathyroidism, deafness, renal dysplasia) syndrome locus maps distal to the DiGeorge syndrome region on 10p13/14. *J. Med. Genet.* **37:** 33–37.
32. Yamagishi, H., Garg, V., Matsuoka, R., Thomas, T., and Srivastava, D. (1999). A molecular pathway revealing a genetic basis for human cardiac and craniofacial defects. *Science* **283:** 1158–1161.
33. Shaikh, T. H., Budarf, M. L., Celle, L., Zackai, E. H., and Emanuel, B. S. (1999). Clustered 11q23 and 22q11 breakpoints and 3:1 meiotic malsegregation in multiple unrelated t(11;22) families. *Am. J. Hum. Genet.* **65:** 1595–1607.
34. Lichter, P., Cremer, T., Borden, J., Manuelidis, L., and Ward, D. C. (1988). Delineation of individual human chromosomes in metaphase and interphase cells by in situ suppression hybridization using recombinant DNA libraries. *Hum. Genet.* **80:** 224–234.